Synthesis and Structural Properties of Patellamide A Derivatives and Their Copper(II) Compounds

Paul V. Bernhardt,[b] Peter Comba,*[a] David P. Fairlie,[c] Lawrence R. Gahan,[b] Graeme R. Hanson,[d] and Lutz Lötzbeyer[a]

Dedicated to Professor Walter Siebert on the occasion of his 65th birthday

Abstract: The synthesis, characterization and copper(II) coordination chemistry of three new cyclic peptide ligands, PatJ[1] (*cyclo*-(Ile-Thr-(Gly)Thz-Ile-Thr-(Gly)Thz)), PatJ[2] (*cyclo*-(Ile-Thr-(Gly)Thz-(D)-Ile-Thr-(Gly)Thz)), and PatL (*cyclo*-(Ile-Ser-(Gly)Thz-Ile-Ser-(Gly)Thz)) are reported. All of these cyclic peptides and PatN (*cyclo*-(Ile-Ser-(Gly)Thz-Ile-Thr-(Gly)Thz)) are derivatives of patellamide A and have a [24]azacrown-8 macrocyclic structure. All four synthetic cyclic peptides have two thiazole rings but, in contrast to patellamide A, no oxazoline rings. The molecular structure of PatJ[1], determined by X-ray crystallography, has a saddle conformation with two close-to-coparallel thiazole rings, very similar to the geometry of patellamide D. The two coordination sites of PatJ[1] with thiazole-N and amide-N donors are each well preorganized for transition metal ion binding. The coordination of copper(II) was monitored by UV/Vis spectroscopy, and this reveals various (meta)stable mono- and dinuclear copper(II) complexes whose stoichiometry was confirmed by mass spectra. Two types of dinuclear copper(II) complexes, $[Cu_2(H_4L)(OH_2)_n]^{2+}$ ($n = 6$, 8) and $[Cu_2(H_2L)(OH_2)_n]$ ($n = 4$, 6; L = PatN, PatL, PatJ[1], PatJ[2]) have been identified and analyzed structurally by EPR spectroscopy and a combination of spectra simulations and molecular mechanics calculations (MM-EPR). The four structures are similar to each other and have a saddle conformation, that is, derived from the crystal structure of PatJ[1] by a twist of the two thiozole rings. The small but significant structural differences are characterized by the EPR simulations.

Keywords: amides · copper · EPR spectrocopy · molecular mechanics · peptides

Introduction

Cyclic peptides are hydrolytically stable and therefore of interest for pharmaceutical applications. Some have been used as efficient enzyme inhibitors, others have antibiotic, antifungal and anticancer activities.[1–8] In nature they are found in bacteria, fungi, and marine organisms.[1–5] The accumulation of various metal ions, in particular of copper(II), by some marine organisms has been related to cyclic peptides[1, 9] but their exact role in the metabolism is still unclear. Metal ion binding to cyclic peptides has been studied in detail and the stabilization of mono- and dinuclear complexes, as well as the selectivity for specific metal ions (mainly copper(II)) have been related to structural constraints, for example by thiazole and oxazoline rings.[10–17] Solid-state and solution structures, and dynamics of metal-free cyclic peptide ligands and of their metal complexes, as well as results of CD and UV/Vis-spectroscopic titrations, have been studied extensively.[1, 9, 13, 18–27] Conformations of the metal-free ligands have been analyzed by crystallography and solution NMR spectroscopy, and related to ring heterocycles and peptide substituents. However, structural data of transition metal compounds of cyclic peptides are still rare and, so far, there is no clear understanding of the unique properties of these compounds as a function of their structure.

Extensive complexation studies with patellamide-type ligands[14, 18, 21, 28] have revealed a number of mono- and dinuclear species in solution. An interesting feature is that, quite generally, two types of dinuclear complexes are observed in slow equilibria (usually a blue and a purple compound), and these were assigned to the slow formation of

[a] Prof. Dr. P. Comba, Dr. L. Lötzbeyer
Anorganisch-chemisches Institut der Universität Heidelberg
Im Neuenheimer Feld 270
69120 Heidelberg (Germany)
Fax: (+49) 6221-54-6617
E-mail: comba@akcomba.oci.uni-heidelberg.de

[b] Dr. P. V. Bernhardt, Prof. Dr. L. R. Gahan
Department of Chemistry
The University of Queensland
Brisbane, Queensland 4072 (Australia)

[c] Dr. D. P. Fairlie
3D Centre, The University of Queensland
Brisbane, Queensland 4072 (Australia)

[d] Prof. Dr. G. R. Hanson
Centre for Magnetic Resonance, The University of Queensland
Brisbane, Queensland 4072 (Australia)

Supporting information for this article is available on the WWW under http://www.wiley-vch.de/home/chemistry/ or from the author.

  0947-6539/02/0807-1527 $ 20.00+.50/0

carbonato-bridged dicopper(II) compounds,[13] to variations in the deprotonation pattern of the ligands and corresponding changes in the donor sets or to partial deprotonation of the aqua coligands.[21] Note that, due to the change in rigidity and ring structure (see below) and due to the differences in donor groups, there might be different species involved with the patellamide group of ligands (ascidiacyclamide, patellamide D, and patellamide A), and those with "hydrolyzed" oxazoline rings (PatN, PatJ[1], PatJ[2], PatL, (see Scheme 1 for ligand structures)): The coordination sites for patellamide-type ligands are $N_{oxazoline}$, N^{-}_{amide}, $N_{thiazole}$, and typical Cu···Cu distances in the dicopper(II) complexes are approximately 4.8 Å ;[13, 18] those for PatN-type ligands are N^{-}_{amide}, N^{-}_{amide}, $N_{thiazole}$ with typical Cu···Cu distances of approximately 5.9 Å.[21]

A combination of empirical force-field calculations with the simulation of dipole-dipole-coupled EPR spectra (MM-EPR[29–32]) has been used previously to determine the first solution structure of a dicopper(II) complex of a synthetic patellamide A derivative, PatN.[21] Solution studies of PatN with copper(II) revealed three mononuclear and two dinuclear complexes in partially slow equilibria, with the most thermodynamically stable species being the purple dinuclear compound $[Cu_2(H_2PatN)(OH_2)_n]$ ($n = 4, 6$).[21]

Herein we present 1) the preparation and characterization of three new derivatives of patellamide A, PatJ[1], PatJ[2], and PatL (Scheme 1), together with the X-ray crystal structural analysis of PatJ[1]; 2) an analysis (UV/Vis, CD, EPR titrations, MS spectra) of the solution equilibria involving the formation of copper(II) complexes with the three new ligands; and 3) a detailed structural analysis of the thermodynamic dicopper(II) products of all four synthetic cyclic peptides (PatN, PatJ[1], PatJ[2] and PatL), based on an improved EPR simulation technology[33–35] and a thorough conformational analysis.[36]

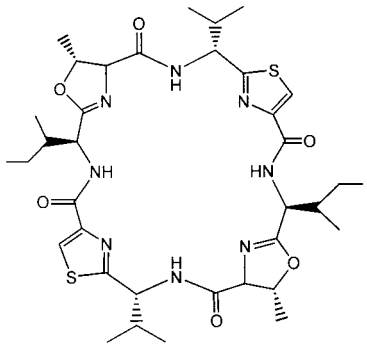

Ascidiacyclamide

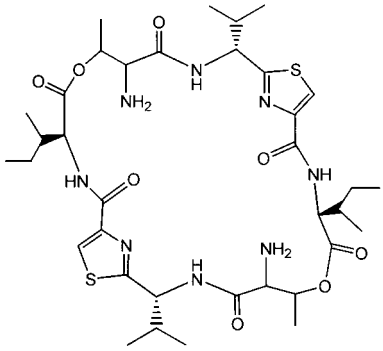

hydrolysed Ascidiacyclamide

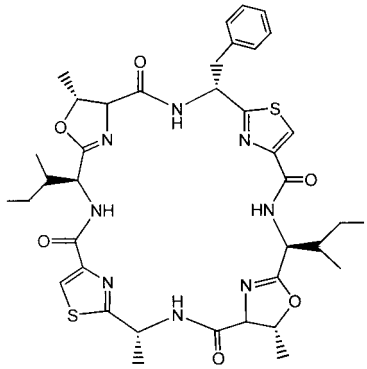

Patellamide D

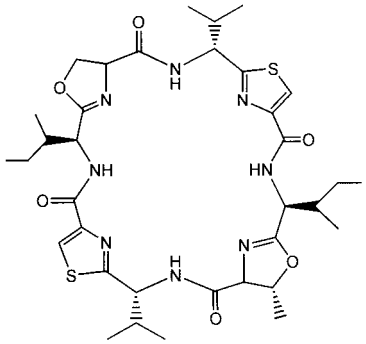

Patellamide A

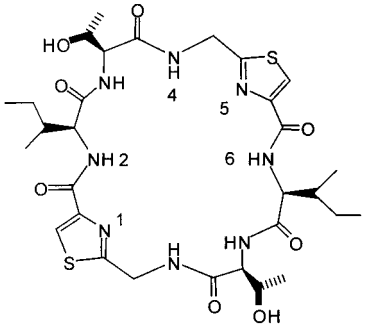

PatJ[1]

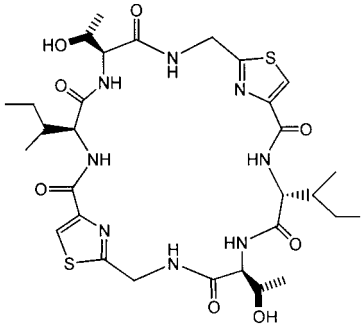

PatJ[2]

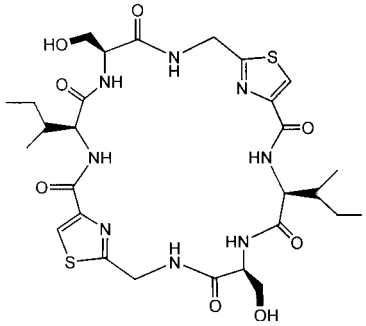

PatL

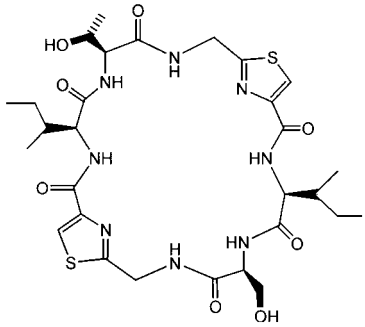

PatN

Scheme 1.

0947-6539/02/0807-1528 $ 20.00+.50/0 *Chem. Eur. J.* **2002**, *8*, No. 7

Results and Discussion

Ligand syntheses and properties: The four cyclic peptide ligands PatN, PatJ[1], PatJ[2], and PatL (*cyclo*-(Ile-Ser-(Gly)Thz-Ile-Thr-(Gly)Thz), *cyclo*-(Ile-Thr-(Gly)Thz-Ile-Thr-(Gly)Thz), *cyclo*-(Ile-Thr-(Gly)Thz-(D)-Ile-Thr-(Gly)Thz), *cyclo*-(Ile-Ser-(Gly)Thz-Ile-Ser-(Gly)Thz), respectively) are all based on the two linear tetrapeptides Ile-Ser-(Gly)Thz and Ile-Thr-(Gly)Thz. The linear octapeptides were prepared by solid-phase synthesis; the key steps are the preparation of the thiazole fragment (Gly)Thz and the cyclization procedure, and these were done as described previously.[21] PatJ[2] is an epimer of PatJ[1] (racemization of C^{α} of one of the Ile fragments during cyclization), and the separation of the two isomeric products was achieved by HPLC. The epimerization of the peptide upon cyclization is not unexpected, and a similar behavior was observed before.[21] The assignment of the structure of PatJ[2] is based on this observation, and supported by the X-ray structural analysis of PatJ[1], detailed NMR spectra of the four macrocycles, and the observed solution structure of the corresponding dicopper(II) complex (see below). The subtle structure differences between PatJ[1] and PatJ[2] might lead to some understanding of conformational preferences of these ligands and the related stabilities of the coresponding complexes. These aspects have not yet been fully evaluated and are not discussed further here. The three new ligands are well characterized by their elemental analyses, MS (ion-spray, HRMS, FAB$^+$), UV/Vis and CD spectra, and extensive NMR studies (^{1}H, COSY, NOESY; see Experimental Section and Supporting Information). The data are consistent with the proposed connectivities and configurations of the cyclic peptide ligands (see Scheme 1), and these assignments are supported by the crystal structural analysis of PatJ[1] (Figure 1).

The cyclic peptides reported here all have a [24]azacrown-8 macrocyclic structure and contain unusual amino acid residues, with two amino(thiazole) rings, which increase the rigidity of the macrocycle and limit the peptide backbone to a few distinct conformations. The patellamide group of macrocycles have two additional heterocyclic rings, that is, two thiazole and two oxazoline rings (see Scheme 1). This restricts the flexibility to three distinct conformations, usually described as type 1, type 2 (saddle), and type 3 (twisted figure-of-eight).[14, 37] It appears that, at least for the bis-seco(oxazoline)-type ligands (PatN, PatJ[1], PatJ[2], and PatL), this nomenclature is not appropriate because a) the additional flexibility must lead to further stable conformations, and b) the distinction between saddle and figure-of-eight generally depends on the orientation of the structural plot. This emerges from Figure 2, whichs shows the structures of PatJ[1], patellamide D, and the dicopper(II) complex of PatJ[1]. PatJ[1] and patellamide D have very similar geometries for the macrocyclic backbone, and that of Patellamide D was determined as type 3 (figure-of-eight); reasons for this might emerge from Figure 1 A.[14] However, the structure of the dicopper(II) compound of PatN (which is similar to that of PatJ[1]) has been correctly classified as "saddle",[21] and from a comparison of the structures of PatJ[1] and the corresponding dicopper(II) complex, it emerges that the main difference is a twist of the two thiazole planes

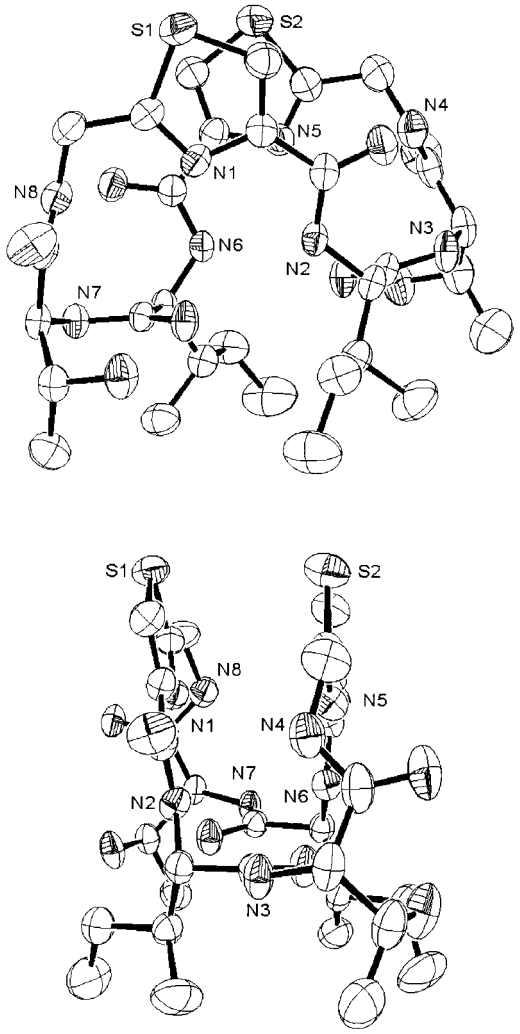

Figure 1. Structure of PatJ[1] (ORTEP plot[43]): A) view perpendicular to thiazole rings, B) view parallel to the thiazole rings.

from approximately 14° to approximately 60°, that is, a partial unfolding of the macrocycle, and PatJ[1] might then also be attributed a saddle structure.

A comparison of the structures of patellamide D[27] and PatJ[1] (see Figure 1 and Figure 2) reveals that in spite of the added flexibility in the ligand backbone of PatJ[1], the solid-state structures of the two cyclic peptides are very similar to each other. The two thiazole rings are roughly coparallel ($\theta^{PatJ^1} = 14°$; $\theta^{PatD} = 8°$), with an average distance of the two aromatic planes of 3.49 Å for PatJ[1] and 3.43 Å for PatD, respectively. The distances of the S atoms of the thiazole rings are 4.02 Å (PaJ[1]) and 4.21 Å (PatD), respectively. The α-amides (each involving Ile) are coplanar with the thiazole rings ($\theta^{PatJ^1} = 4.1°$ and 4.7°; $\theta^{PatD} = 11.2°$ and 11.6°; see N1, N2 and N5, N6 donor sets in Figure 1 A. The other amide substituents (involving Thr) are tilted out of these planes by approx. 120° and 126° for PatJ[1] and PatD, respectively (see N1, N8 and N5, N4 donor stes in Figure 1 A). Therefore, the two putative coordination sites for copper(II) in PatJ[1] (N1, N2, N8 and N5, N6, N4, see Figure 1) are partially preorganized (N1, N2 and N5, N6; see also discussion of the copper(II) structures below).

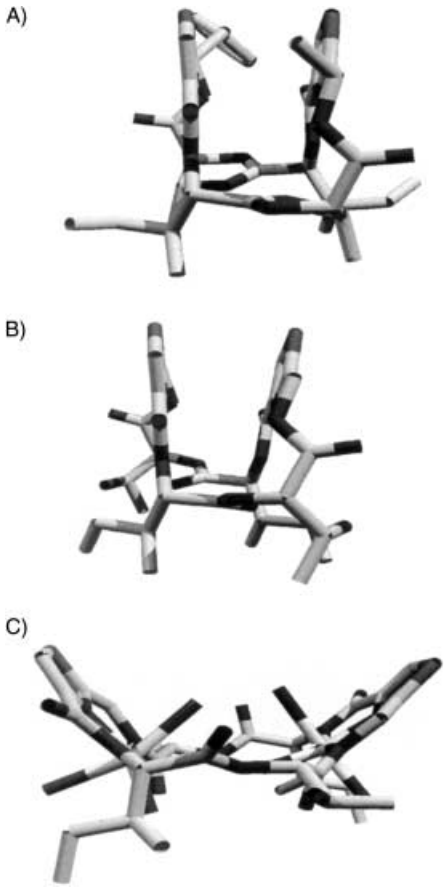

Figure 2. Structures of A) patellamide D,[27] B) PatJ[1] (see Figure 1) and C) $[Cu_2(H_2PatJ^1)(OH_2)_6]$ (see Figure 5).

Copper coordination chemistry: The analysis of the copper(II) coordination chemistry of ascidiacyclamide, patellamide D and PatN (in methanol, due to restricted solubility in water; OH^- or triethylamine as base; one or two equivalents of Cu^{2+}; Cl^-, NO_3^- or ClO_4^- salts) indicated that various mono- and dinuclear species are present in solution (partially slow equilibria).[13, 18–21] The most thorough spectroscopic study is that of PatN, and that revealed a mononuclear complex with a doubly deprotonated ligand ($[Cu(H_4PatN)]$) to be the most stable mononuclear compound, followed by the complex of the monodeprotonated ligand ($[Cu(H_5PatN)]^+$); the most stable species in solution, however, was a purple dinuclear complex ($[Cu_2(H_2PatN)(OH_2)n]$, $n=4$, 6), whose structure was studied by MM-EPR; a less stable dinuclear copper(II) complex was present initially but this was not fully characterized.[21] Spectrophotometric titrations, coupled with EPR and mass spectra, of the three new ligands provide a better understanding of the stoichiometry and geometry of the major copper(II) complexes with this class of bis-seco(oxazoline)-type Patellamide derivatives in solution.

Spectrophotometric titrations were employed to follow the formation of mono and dinuclear complexes as a function of base (up to six equivalents with respect to the ligand). Both $CuCl_2$ and $Cu(ClO_4)_2$ were used as sources of copper. The final solutions were frozen and later used for EPR studies and mass spectrometry. Some of the EPR spectra were measured as a function of time to check for slow changes in the equilibria. The spectrophotometric data reported are corrected for volume changes due to the addition of base. The concentration of PatL was determined by titration with copper(II),[21] whilst those of PatJ[1] and PatJ[2] (analytically pure peptide ligands) were based on weight (see Experimental Section). The data of the spectrophotometric titration experiments are assembled in Table 1 (full data sets are available as Supporting Information), and Figure 3 shows the $[OH^-]_{added}$-dependent spectra of copper(II)/PatJ[1] solutions (plots of titrations with the other ligands are given as Supporting Information). The assignment of the species in solution is supported by the mass spectrometric analyses of the solutions (see Experimental Section). Note, the mass spectra (MS) are dominated by Na^+ adducts (addition of NaOH), and the relative intensity of the signals for the mono and dinuclear copper(II) complexes (unambigiously assigned by the characteristic isotope patterns) are small. Both, blue (Cu:L = 1:1) and purple solutions (Cu:L = 2:1) show MS peaks for CuL and Cu_2L (and corresponding signals for free ligand and Na^+-adducts) but dicopper(II) compounds dominate in the purple solutions (see Experimental Section).

Table 1. UV/Vis titration data of solutions of copper(II) and L (1:1 or 2:1) with OH^-; λ_{max} [nm], ε [$M^{-1}cm^{-1}$].[a]

Cu:L:OH	PatJ[1]		PatJ[2]		PatL	
	λ	ε	λ	ε	λ	ε
1:1:1	660	75	690	70	640	70
1:1:2 (comp. A,B,C)	580	230	585	180	585	160
1:1:4 (comp. B)	550	190	540	210	560	120
2:1:1	680	60	720	120	660	60
2:1:2	590	150	560	200	580	380
2:1:4 (comp. D)	560	740	550	420	570	200
2:1:6 (comp. D)	540	480	530	400	560	200

[a] For the accuracy of ε see Experimental Section.

The general observation is that the dd transition of free, solvated copper(II) at around 800 nm is shifted to approximately 660 nm (experiments $Cu:L:OH^- = 1:1:1$, metastable species; here and in the following discussion of the spectroscopic data we use PatJ[1] as the example; note that PatJ[2], PatL (and PatN) give qualitatively very similar spectra; see Table 1). Based on earlier studies,[21] the stoichiometry of the solutions, the MS data, the EPR data (see below) and the structural observations (see above), this species is assumed to be $[Cu(H_5L)(OH_2)_n]^+$, $n=3$, 4 (five- or six-coordinate copper(II) site). Based on the crystal structure of the metal-free ligand, we assume that one of the α-amides (with respect to the thiazole residue), that is, that in-plane with the thiazole donor (Ile), is deprotonated and the copper(II) center is coordinated to the highly preorganized bidentate thiazole-N-amide site. Addition of a second equivalent of base leads to deprotonation of a second amide site and coordination of the peptide as a tridentate ligand, to form the mononuclear species $[Cu(H_4L)(OH_2)_n]$, $n=2$, 3 (five- or six-coordinate copper(II) site), with an electronic transition at approximately 550 nm (high-energy shift expected due to the stronger ligand field). This species is in a slow equilibrium with the corresponding dinuclear product and free ligand (free ligand is included in Scheme 2 only as H_6L; see below).

0947-6539/02/0807-1530 $ 20.00+.50/0 *Chem. Eur. J.* **2002**, *8*, No. 7

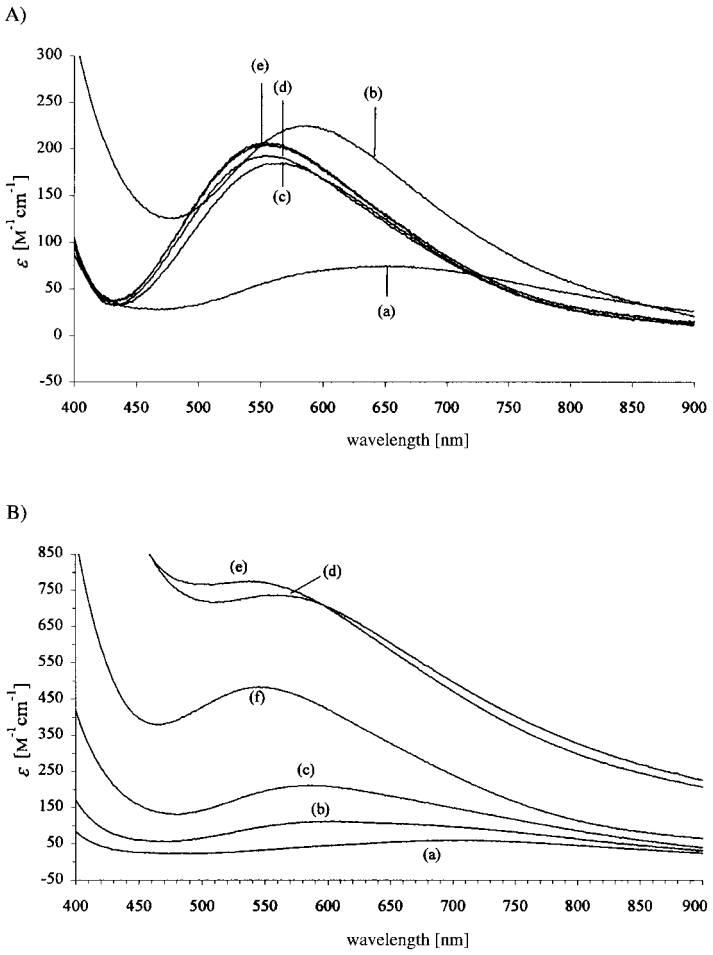

Figure 3. A) Spectrophotometric titration data of PatJ[1] ($Cu(ClO_4)_2$:L = (1:1); a), b), c), d), and e) addition of 1, 2, 3, 4, and 6 equiv base (curves for 5 and 6 equiv are equivalent); note that the titrations of PatJ[1] $CuCl_2$:L = (1:1) with up to 6 equiv base and $Cu(ClO_4)_2$:L = (1:1) with up to 2 equiv base led to identical results; note that the accuracy of ε is only approximately ±15% (see Experimental Section). B) Spectrophotometric titration data of PatJ[1] $Cu(ClO_4)_2$:L = (2:1); a), b), c), d), e), and f): addition of 1, 2, 3, 4, 5, and 6 equiv base; note that the titration of PatJ[1] $CuCl_2$:L = (2:1) with up to 6 equiv of base is identical to that shown here; note that the accuracy of ε is only approximately ±15% (see Experimental Section).

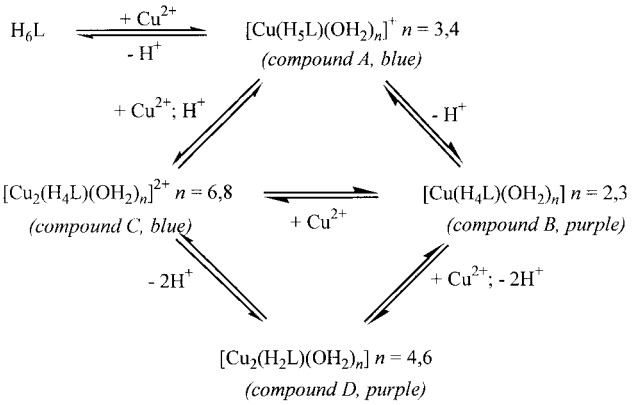

Scheme 2.

Two species with distinct electronic spectra are observed in experiments with a Cu:L ratio of 2:1. After addition of two equivalents of base a species with a transition at approximately 590 nm is formed, with an additional two equivalents of base, the final spectrum has a maximum at approximately 540 nm. The extinction coefficients in comparison with those of the titration with a Cu:L ratio of 1:1 indicate that the latter species is dinuclear, and from the transition energies it appears that the mononuclear (see above) and dinuclear compounds have similar chromophores. Spectroscopic changes in the region of the ligand transitions ($\pi \rightarrow \pi^*$ (thiazole rings), ca. 220 nm; $n \rightarrow \pi^*$ (conjugated thiazole/carbonyl fragments), ca. 310 nm), and of the CD spectra (positive Cotton effect at ca. 330 nm) are consistent with the proposed species, but poor spectral resolution precludes a thorough analysis.

EPR spectra (frozen solutions) of the solutions from experiments with Cu:L:OH^- ratios of 1:1:2 (fresh, and aged for PatJ[1]) and 2:1:6 were also used to analyze the species present in solution. The corresponding data are presented in Table 2 and Figure 4 (plots of the experimental and simulated EPR spectra of PatJ[2], PatL and PatN are given as Supporting Information). The simulated spectra are the result of optimization procedures implemented in Sophe. Sophe[33, 34] creates the full Hamiltonian matrix from the g and copper hyperfine matrices for the isolated copper(II) centers and the dipole–dipole interactions. Also, Sophe includes a *g* and *A* strain line width model. Therefore, the spin-Hamiltonian parameters represent the chromophores alone, and those of the mono and dinuclear species are directly comparable. It follows that the parameters reported in the earlier study with PatN,[21] analyzed by DISSIM,[38] are not directly comparable

Table 2. EPR parameters for mononuclear and dinuclear copper(II) complexes of PatJ1, PatJ2, and PatL.

	PatJ1	PatJ2	PatL	PatN
Compd A, mononuclear[a]				
$g\perp$	2.063	2.064	2.062	2.061
$g\parallel$	2.240	2.346	2.331	2.240
$A\perp$ [10^{-4} cm^{-1}]	25.8	24.12	22.5	25.0
$A\parallel$ [10^{-4} cm^{-1}]	111.8	129.1	130	112
Compd C, dinuclear[b]				
$g\perp$	2.063	2.067	2.073	2.057
$g\parallel$	2.227	2.229	2.221	2.23
$A\perp$ [10^{-4} cm^{-1}]	36.5	26.5	26.5	40
$A\parallel$ [10^{-4} cm^{-1}]	111.5	108.5	106.5	109
r [Å]	6.34	6.01	6.09	6.33
ξ [°]	22.5	21.5	17.8	16.5
τ [°]	3.5	4.93	7.1	4
η [°]	5	4.85	15.1	9
Compd D, dinuclear[c, d]				
$g\perp$	2.025	2.05	2.09	2.089
$g\parallel$	2.201	2.226	2.253	2.260
$A\perp$ [10^{-4} cm^{-1}]	55	59	35	77
$A\parallel$ [10^{-4} cm^{-1}]	79	72.5	87.5	82
r [Å]	5.85	5.75	5.85	5.89
ξ [°]	60	42	29	88
τ [°]	75	85	79	35
η [°]	80	30	31	25

[a] Computer simulation for the Cu:L = (1:1) experiment, 2 equiv base, mononuclear species. [b] Computer simulation for the Cu:L = (1:1) experiment, 2 equiv base, dinuclear species. [c] Computer simulation for the Cu:L = (2:1) experiment, 6 equiv base, dinuclear species. [d] A mononuclear species (compd B) with similar electronic parameters was also simulated, see text and Figure 4 A.

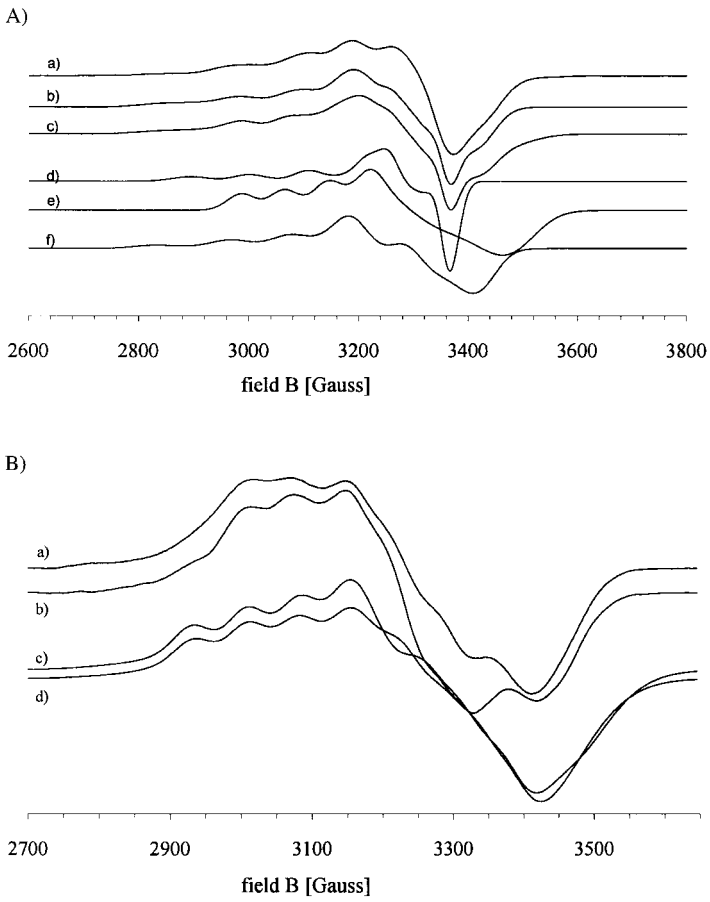

Figure 4. A) Experimental X-band EPR spectrum of the blue copper(II)-PatJ^1 solutions (Cu^{II}:L = 1:1; 2 equiv base) at $\tilde{\nu} = 9.573$ GHz, 130 K; a) experimental spectrum, b) sum of the computer simulation of the mononuclear complex (d) and the dinuclear complex (f) (approx. 1:1), c) sum of the computer simulation of the two mononuclear complexes (d) and (e) (blue and purple chromophores, see text) and the dinuclear complex (f) (ca. 0.75:0.25:1). B) Experimental X-band EPR spectrum of the purple copper(II) solutions of PatJ^1 at $\tilde{\nu} = 9.442$ GHz, 130 K; a) L:Cu^{II} (1:1), 6 eqiuiv base; b) L:Cu^{II} (1:2), 6 equiv base; c) XSophe computer simulation of (a) and (b), d) computer simulation with MOMEC structural parameters based on PatJ^1–1.

with those given here, and the earlier analysis of the spectra of solutions with various compounds in equilibrium was, due to restrictions in the simulation technology, less accurate than that presented here.

From the simulation of the EPR spectra it emerges that three species dominate the equilibria (see Table 2): EPR spectra of the blue solutions resulting from a Cu:L:OH^- of 1:1:2 ($\lambda_{max} \approx 580$ nm, $\varepsilon \approx 230\ l\,mol^{-1}\,cm^{-1}$, see Table 1) can only be simulated as the sum of a mono- and a dinuclear compound (ca. ratio 1:1). The two species have similar chromophores, as expected from the UV/Vis data, $\lambda_{max} \approx 580$ nm (PatJ^1: $g_\perp = 2.06$, $g_\parallel = 2.23$, $A_\parallel = 112 \times 10^{-4}\,cm^{-1}$; there are some variations within the set of three ligands, see Table 2). The purple solutions (Cu:L:$OH^- = 2:1:6$; $\lambda_{max} \approx 540$ nm, $\varepsilon \approx 480\ l\,mol^{-1}cm^{-1}$, see Table 1) are pure dinuclear compounds with a significantly different chromophore (PatJ^1: $g_\perp = 2.03$, $g_\parallel = 2.20$, $A_\parallel = 79 \times 10^{-4}\,cm^{-1}$). Also, the structural parameters of the two dinuclear compounds are significantly different, for example, Cu $\cdots$ Cu is approximately 6.3 Å for the blue and approximately 5.9 Å for the purple compound (see Table 2). Thus, it appears that the second deprotonation of the cyclic peptides studied here, leading to H_4L, occurs at the second coordination site and leads to the formation of dinuclear complexes (and free ligand). Addition of more base converts this metastable species with bidentate bonding of the macrocycle to the stable, purple product with two copper(II) ions coordinated to the thiazole nitrogen donors and two deprotonated amides, each. This analysis (see Scheme 2) is consistent with the UV/Vis, the MS, and EPR data, if two mononuclear complexes with different colors, that is, due to H_5L and H_4L, see electronic spectra, and two complexes of H_4L, that is mono- and dinuclear are allowed. The shift of the electronic transition from approximately 660 nm to approximately 580 nm in the blue Cu:L = 1:1 solutions upon addition of a second equivalent of base (see above) indicates the coordination of a second amide donor (see above). This shift is smaller than that in the titration of the Cu:L = 2:1 solution, where the electronic transitions after addition of six equivalents of base reach values of approximately 540 nm. Thus, the blue solutions (Cu:L:OH = 1:1:2) are believed to consist of $[Cu(H_5L)(OH_2)_n]^+$ (≈ 660 nm, $A_\parallel \approx 112 \times 10^{-4}\,cm^{-1}$), $[Cu(H_4L)(OH_2)_n]$ (≈ 550 nm, $A_\parallel \approx 79 \times 10^{-4}\,cm^{-1}$), and $[Cu_2(H_4L)(OH_2)_n]^{2+}$ (≈ 660 nm, $A_\parallel \approx 112 \times 10^{-4}\,cm^{-1}$). The broad dd transitions clearly preclude a deconvolution into various transitions and considerable overlap of the EPR signals does not lead to any significant improvement when three instead of two species are used in the simulations (see Figure 4).

Solution structures of the purple dinuclear products: The structural analysis by the MM-EPR approach[21, 29] involves a full conformational search, based on a random kick module, implemented in MOMEC97[36, 39] (see Experimental Section for details), followed by a full optimization of the lowest energy structures (ca. 15–30 structures for each of the species analyzed),[21, 40] and the EPR simulation with the structural parameter sets obtained from each of the lowest energy optimized structures. The molecular mechanical structure optimization is based on harmonic bonding potentials and, therefore, the coordination number is fixed, while the coordination geometry is flexible, due to the replacement in MOMEC of the harmonic valence angle bending potentials by 1,3-nonbonded interactions around the metal center. While for the purple dinuclear complexes there are structural analogues and the complexes are rather rigid, there are large numbers of very flexible isomers for the blue compounds with bidentate coordination of the peptides to the copper(II) center. Therefore, we concentrate on the structure determination of the more stable thermodynamic products. These were optimized as six-coordinate complexes; five-coordination leads to similar, although slightly less convincing results.

The Euler angles ξ, τ, and η, which are needed for the EPR spectral simulations, together with the Cu $\cdots$ Cu distance, the linewidth, the g and A strain and the spin Hamiltonian parameters (g and A values). Reasonably accurate starting values for the electronic parameters were obtained from the spectra of the mononuclear compounds. The geometric parameters (r, ξ, τ, η) define the orientation of the two g

  0947-6539/02/0807-1532 $ 20.00+.50/0 *Chem. Eur. J.* **2002**, *8*, No. 7

matrices and these need not coincide exactly with the molecular coordinate system. More importantly, the definition of a molecular coordinate system in highly unsymmetrical hexacoordinate compounds such as those reported here (see Figure 5) is not unambiguous (in order to facilitate a comparison between the set of four structures discussed here, the measurement of the Euler angles in the force-field-optimized structures was done in a consistent way (see Experimental Section). Nevertheless, there are significant deviations between the structural parameters from the EPR simulation and from the MM-EPR analysis (see Table 3). These might be the results of ambiguities in the measurement of the geometric parameters from the strain-energy-minimized structures[21, 40] (see above), small inconsistencies in the force field used, the neglect of solvation, and some inconsistencies in the EPR spectral simulations might also contribute to the limited accuracy. The structural results are listed in Table 3 and the optimized structures are presented in Figure 5.

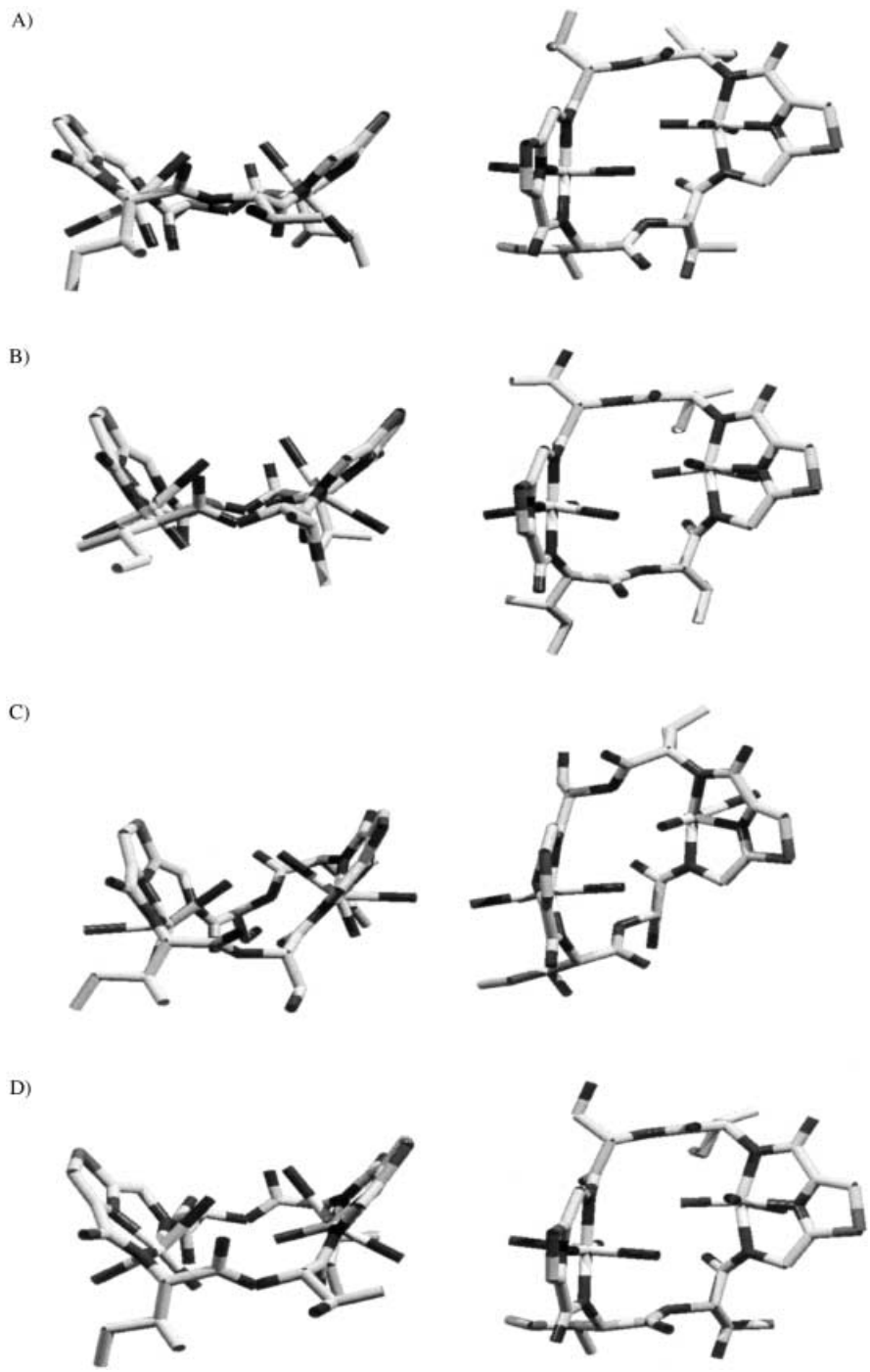

Figure 5. Two views each for the computed structures (MM-EPR) of the purple dicopper(II) complexes of $PatJ^1$ (A), $PatJ^2$ (B), PatL (C) and PatN (D).

Conclusion

The [24]azacrown-8 macrocyclic peptide ligands $PatJ^1$, $PatJ^2$, PatL, and PatN, derivatives of patellamide A with open oxazoline rings, form stable dicopper(II) compounds. The molecular structure of the metal-free peptide $PatJ^1$ indicates that, due to the constraints by the thiazole rings, the ligands are well preorganized for metal uptake. This is believed to be the reason for the stability of the dicopper(II) complexes. The solution structural studies indicate that metal ion coordination leads to a flattening of the ring, mainly due to repulsion of the extra ligands (coordinated water molecules in the present case).

The fact that the titration of Cu^{II}:L in ratios 1:1 and 2:1 with base leads to mixtures of mono- and dinuclear compounds indicates that the dicopper(II) compounds are more stable than the initially formed mononuclear species. The various forms of dicopper(II) complexes are believed to be related by protonation/deprotonation processes, with the purple form $[Cu_2(H_2L)]$ with four deprotonated amides being the most stable compound in the system. The shift of color for the mono- and dinuclear complexes (blue to purple) is consistent with an increasing ligand field upon deprotonation and coordination of additional amide sites. All dicopper(II) species analyzed structurally in this study are rather similar saddle-shaped dicopper(II) complexes with differences mainly due to the conformations of the peptide spacer groups between the two coordination sites. The combination of EPR spectroscopy with molecular modeling is a valuable tool to analyze these variations.

Table 3. Angles, Cu ··· Cu distances, and strain energies of the calculated structures (six lowest energy minima, 1 to 6[a]), compared with the parameters from the EPR simulation (see Table 2) of the purple dinuclear Cu^{II} complexes of PatJ[1], PatJ[2], PatL, and PatN.

	Strain energy [kJ mol^{-1}]	r [Å]	ξ [°]	τ [°]	η [°]
PatJ[1]		5.85	60	75	80
PatJ[1] – 1	*78.31*	*5.70*	*57*	*82*	*76*
PatJ[1] – 2	85.57	5.55	50	74	86
PatJ[1] – 3	87.23	5.56	48	87	69
PatJ[1] – 4	87.46	5.82	51	73	83
PatJ[1] – 5	87.96	5.63	50	72	88
PatJ[1] – 6	87.96	5.94	46	79	77
PatJ[2]		5.75	42	85	30
PatJ[2] – 1	*79.05*	*5.58*	*37*	*86*	*70*
PatJ[2] – 2	81.76	5.66	48	80	94
PatJ[2] – 3	82.90	5.51	41	83	64
PatJ[2] – 4	84.01	5.61	39	90	70
PatJ[2] – 5	87.47	5.94	54	79	83
PatJ[2] – 6	88.31	5.75	61	72	93
PatL		5.85	29	79	31
PatL – 1	*75.92*	*5.93*	*41*	*82*	*43*
PatL – 2	76.39	5.72	49	80	74
PatL – 3	77.26	5.68	48	83	72
PatL – 4	77.27	5.52	48	85	79
PatL – 5	79.08	5.87	49	84	53
PatL – 6	85.54	5.63	61	87	91
PatN[b]		5.89	88	35	25
PatN[c]		5.75	55	37.5	30
PatN – 1	*76.04*	*6.21*	*65*	*62*	*93*
PatN – 2	77.75	5.51	51	89	72
PatN – 3	78.20	5.62	54	84	78
PatN – 4	79.82	5.64	57	82	75
PatN – 5	80.11	5.37	51	65	87
PatN – 6	80.19	5.26	65	62	93

[a] Lowest energy structure 1 in italics. [b] See Table 2. [c] Taken from reference [21].

Experimental Section

Measurements: All reagents and solvents were of analytical grade and used without further purification. ^{1}H and ^{13}C NMR spectra were recorded with either Bruker WH 300, Varian 300 MHz, Bruker AMX 500 or Bruker Avance DRX 500 spectrometers; chemical shifts are reported relative to TMS or solvent internal standards.

Preparative scale reversed-phase (rp) HPLC separations were performed on a Waters Delta-Pak PrepPak C_{18} 40 × 100 mm cartridge (100 Å). Linear peptides were purified using gradient mixtures of water (0.1 % TFA, solvent system A) and 10 % water · 90 % CH_3CN · 0.1 % TFA (solvent system B). Cyclic peptides were purified using gradient mixtures of water and CH_3CN (100 % solvent system A to 100 % solvent system B).

UV/Vis spectra were recorded with a Perkin Elmer Lamda 40 spectrometer. The accuracy of the ε values is, due to volumetric inaccuracies (copper(II) and peptide concentrations, addition of base, small samples) of the order of ± 15 %. Circular dichroism (CD) spectra were recorded with a JASCO J-710 spectropolarimeter. The measurements (200 – 800 nm at room temperature) were carried out in MeOH, using cells with 0.1 cm path length. Mass spectra were obtained with a Mariner Biospec Electrospray Time of Flight (ES/TOF MS) mass spectrometer (Applied Biosystems, Framingham, USA). The infusion flow rate was 60 µL min^{-1}, typical injection volumes are 20 µL. The declustering voltages Skimmer 1, Skimmer 2 and Nozzle potential were typically 60, 30, and 10 V, respectively. Data was processed using the Biospec application programme. High-resolution mass spectra were recorded with an internal standard, using reserpine purchased from Sigma.

Electron paramagnetic resonance spectra (EPR) were recorded with a Bruker ESP 300 E EPR or a Bruker ELEXSYS E 500 EPR spectrometer, equipped with an EIP 548 B microwave frequency counter and a Bruker E 035 M Gauss meter for microwave frequency and magnetic field calibration. A flow-through cryostat in conjunction with a Euroterm (B-VT-2000) variable temperature controller provided temperatures of 120 – 140 K at the sample position in the cavity. Helium temperatures (1.9 – 4 K) were obtained using a CF-935 cryostat in conjunction with an Oxford Instruments ITC-4 temperature controller. EPR computer simulations were done with XSophe, version 1.0.2β, on an SGI O2-workstation, using a distribution of g and A values line width model. Frequencies and temperatures are given in the figure captions.

Conformational analyses were performed with the MOMEC 97[39] program and force field,[21, 36, 40] using the random kick stochastic searching module.[36] To scan the conformational space in each structure, six individual structures were generated based on the EPR simulation parameters. For each structure 1000 kicks were allowed, with a maximum atom shift of 3 Å (random orientation). Full optimization was done for all low energy structures (within 10 kJ mol^{-1} from the global energy minimum). For the definition of the geometric parameters for the EPR simulations the biggest problem was the definition of the xy plane of the two copper sites. This was done in a consistent way, using the thiazole-N and the two amide-N donors, as well as the copper center; the z axis was assumed to be perpendicular to this plane.

For X-ray crystallography, the single crystal was mounted on glass fibers with Supa glue. Lattice parameters were determined by least-squares fits to the setting parameters of 25 independent reflections, measured and refined on an Enraf-Nonius CAD 4 diffractometer, using graphite-monochromated $Mo_{K\alpha}$ radiation. The structure was solved by heavy-atom and direct methods, and refined using full-matrix least squares on F^2. Programs used were SHELX[41] and SHELXL-93[42] for solution and refinement, respectively, and ORTEP[43] for plotting. Crystallographic data are assembled in Table 4.

Syntheses

Boc-Gly(Thz)-OH: HBr · H_2N-Gly(Thz)-OMe (3.48 g; 13.75 mmol) was dissolved in THF/$H_2$0 (20 mL; 1:1) and left stirring at 0 °C. LiOH · $H_2$0 (1.735 g, 41.25 mmol) was added and the reaction mixture left stirring for one hour. The *tert*-butyloxycarbonyl (Boc) protecting group (3.00 g, 13.75 mmol) was added and the solution warmed up to room temperature and left stirring for 12 hours. The organic solvent was removed in vacuo and the aqueous layer acidified to pH 3. The aqueous layer was extracted with acetic acid. The solvent was removed in vacuo; yield: 2.21 g (93.47 %).

Table 4. Crystal data and structure refinement for PatJ[1].

empirical formula	$C_{30}H_{46}N_8O_9S_2$
formula weight	726.87
temperature [K]	293(2)
wavelength [Å]	0.71073
crystal system	monoclinic
space group	$P2(1)$
unit cell dimensions	
a [Å]	11.194(3)
b [Å]	10.1010(1)
c [Å]	16.593(4)
β [°]	104.22(1)
volume [Å^3]	1818.7(7)
Z	2
ρ_{calcd} [Mg m^{-3}]	1.327
absorption coefficient [mm^{-1}]	0.208
$F(000)$	772
crystal size [mm]	0.6 × 0.5 × 0.5
θ range [°]	1.88 – 24.98
index ranges	$0 \le h \le 13$, $0 \le k \le 12$, $-19 \le l \le 19$
reflections collected	3565
independent reflections	3383 [R(int) = 0.0176]
refinement method	full-matrix least-squares on F^2
data/restraints/parameters	3383/1/444
goodness-of-fit on F^2	1.025
final R indices [$I > 2\sigma(I)$]	$R1 = 0.0334$, w$R2 = 0.0871$
R indices (all data)	$R1 = 0.0471$, w$R2 = 0.0946$
absolute structure parameter	0.05(9)
largest difference peak and hole [e Å^{-3}]	0.269 and −0.214

0947-6539/02/0807-1534 $ 20.00+.50/0 *Chem. Eur. J.* **2002**, *8*, No. 7

^{1}H NMR (500 MHz, [D$_6$]DMSO): $\delta = 1.41$ (s, 9H; $(CH_3)_3$C-), 4.38, 4.39 (d, ^3J(H,H) = 6.0 Hz, 2H; CH_2-Gly), 7.82 (t, 1H; NH-Gly), 8.32 (s, 1H; CH-Thz); ^{13}C NMR (75 MHz, DMSO) $\delta = 28.17$ ((CH_3)C-), 41.94 (CH_2-Gly), 78.70 ((CH_3)C-), 128.45 (CH-Thz), 146.96, 155.78 (2 × C-Thz), 162.11, 171.53 (CO-Boc, COOH); ESMS: *m*/*z* (%): 259.0 (100) $[M+H]^+$ (calcd 258.3).

H-(Thr-Gly(Thz)-Ile-Thr-Gly(Thz)-Ile)-OH: Boc-Ile-PAM resin (0.67 g, substitutional value = 0.746 mmol g^{-1}) was deprotected with trifluoroacetic acid (TFA; 5 mL, 2 × 2 min), washed with DMF, and a solution of Boc-Gly(Thz)-OH (0.26 g; 2 equiv), 2-(1*H*-benzotriazol-1-yl)-1,1,3,3-tetramethyluronium-hexafluorophosphate (HBTU; 0.5 M in DMF 2 mL) and diidsopropylethylamine (DIPEA; 0.47 mL) was added. The reaction mixture was shaken for 20 min, and the reaction monitored by the negative ninhydrin test (>99.5% coupling). The phenylacetamidomethyl (PAM) resin was washed with DMF and the synthesis completed by the sequential coupling of Boc-Thr(OBzl)-OH (4 equiv), Boc-Ile-OH (4 equiv), Boc-Gly(Thz)-OH (2 equivuiv), and Boc-Thr(OBzl)-OH (4 equiv), using the same procedure, and finally washed with DMF, MeOH, MeOH/CH_2Cl_2 (1:1). The peptide was cleaved from the resin with HF at −5 to −1 °C with 1 mL *p*-cresol as scavenger for the protecting benzyl groups, precipitated and washed several times using diethyl ether, redissolved in water acetonitrile (1:1) and lyophilized. The crude powder was purified by HPLC (gradient, 60 min) to give H-(Thr-Gly(Thz)-Ile-Thr-Gly(Thz)-Ile)-OH as a white powder; yield: 220.3 mg (60.6%). ^{1}H NMR (500 MHz; DMSO): $\delta = 0.79$, 0.81, 0.82 (t, ^3J(H,H) = 7.5 Hz, 7.5 Hz, 3H; δ-CH_3-Ile), 0.85, 0.87, 0.88 (t, ^3J(H,H) = 7.0 Hz, 6.0 Hz, 3H; δ-CH_3-Ile), 1.05, 1.06 (d, ^3J(H,H) = 6.0 Hz, 3H; γ-CH_3-Ile), 1.12, 1.13 (d, ^3J(H,H) = 6.5 Hz, 3H; γ-CH_3-Ile), 1.05, 1.06 (d, ^3J(H,H) = 6.0 Hz, 3H; CH_3-Thr), 1.12, 1.13 (d, ^3J(H,H) = 6.5 Hz, 3H; CH_3-Thr), 1.10–1.21 (m, 4H; 2 × γ-CH_2-Ile) 1.44–1.53 (m, 1H; β-CH-Ile), 1.87–1.91 (m, 1H; β-CH_3-Ile), 3.87–3.92 (m, 1H; β-CH-Thr), 3.98–4.02 (m, 1H; β-CH-Thr), 4.23–4.31 (m, 2H; α-CH-Thr), 4.47–4.71 (m, 6H; 2 × α-CH-Ile, 2 × CH_2-Gly), 7.92, 7.94 (d, ^3J(H,H) = 8.5 Hz, 1H; NH-Thr), 8.09, 8.11 (d, ^3J(H,H) = 9.5 Hz, 1H; NH-Ile), 8.15, 8.18 (2s, 2H; CH-Thz), 8.21, 8.23 (d, ^3J(H,H) = 8.5 Hz, 1H, NH-Thr), 8.67, 8.70, 8.71 (t, ^3J(H,H) = 6.0 Hz, 5.5 Hz, 2H; NH-Gly), 9.20 (brs, 1H; NH-Ile); ^{13}C NMR (300 MHz; DMSO): $\delta = 10.89$, 11.62 (2 × γ-CH_3-Ile), 15.43, 15.72 (2 × δ-CH_3-Ile), 20.15 (2 × CH_3-Thr), 24.40, 25.02 (2δ-CH_2-Ile), 37.05, 37.40, 38.44, 38.46 (2 × β-CH-Ile, 2 × CH_2-Gly), 57.04, 57.18, 58.57, 58.59 (2 × α-CH-Ile, 2 × α-CH-Thr), 66.45, 66.66 (2 × β-CH-Thr), 124.25, 124.60 (2 × CH-Thz), 148.82, 149.01, 159.58, 159.84 (4 × C-Thz), 169.84, 169.99, 170.56, 170.82, 170.85, 173.00 (6 × CO); ESMS: *m*/*z* (%): 727.3 (100) $[M+H]^+$ (calcd 726.9).

***cyclo*(Ile-Thr-Gly(Thz))$_2$, PatJ^1, PatJ^2**: A solution of H-(Thr-Gly(Thz)-Ile-Thz-Gly(Thz)-Ile)-OH (100 mg, 0.14 mmol), [benzo-triazol-1-yloxytris-(dimethylamino)phosphonium]hexafluorophosphate (BOP; 186 mg, 0.42 mmol) and DIPEA (90 mg, 0.7 mmol) in DMF (150 mL) was stirred at room temperature for one hour; the reaction was monitored by mass spectrometry. The solvent was evaporated in vacuo and the residue purified by HPLC (gradient, 60 min). The appropriate fractions were combined and lyophilized to give *cyclo*(Ile-Thr-Gly(Thz))$_2$, PatJ^1; yield: 27.84 mg (28.1%) and *cyclo*(L-Ile-Thr-Gly(Thz)-D-Ile-Thr-Gly(Thz)), PatJ^2; yield: 21.82 mg (22.0%). PatJ^1: ^{1}H NMR (500 MHz, [D$_3$]MeOH): $\delta = 0.89$, 0.90, 0.92 (t, ^3J(H,H) = 7.5, 7.0 Hz, 6H; 2δ-H_3-Ile), 1.06, 1.07 (d, ^3J(H,H) = 7.0 Hz, 6H; 2γ-CH_3-Ile), 1.17–1.28 (m, 2H; γ-CH_2-Ile), 1.25, 1.26 (d, ^3J(H,H) = 6.5 Hz, 6H; 2CH_3-Thr), 1.69–1.75 (m, 2H; γ-CH_2-Ile), 2.38–2.39 (m, 2H; β-CH-Ile), 4.03 (brs, 2H; α-CH-Thr), 4.17–4.20 (m, 2H; α-CH-Ile), 4.35–4.38 (m, 2H; CH_2-Gly), 4.69 (m, 2H; β-CH-Thr), 5.10–5.12 (m, 2H; CH_2-Gly), 7.66 (s, 2H; CH-Thz), 8.25, 8.27 (d, ^3J(H,H) = 7.5 Hz, 2H; NH-Gly), 9.11, 9.12 (d, ^3J(H,H) = 5.5 Hz, 2H; NH-Ile), 9.45 (brs, 2H; NH-Thr); ESMS: *m*/*z* (%): 709.3 (100) $[M+H]^+$; HRMS: 709.27523, calcd for $C_{30}H_{45}N_8O_8S_2$: 709.28018; elemental analysis calcd (%) for $C_{30}H_{44}N_8O_8S_2 \cdot 2H_2O$: C 48.23, H 6.50, N 15.04; found: C 48.23, H 6.27, N 15.15; retention time for analytical HPLC (gradient, 32 min.): 18.8 min. PatJ^2: ^{1}H NMR (500 MHz, [D$_3$]MeOH): $\delta = 0.89$, 0.91, 0.92 (t, ^3J(H,H) = 7.5 Hz, 7.5 Hz, 3H; δ-CH_3-Ile), 0.98, 0.99, 1.01 (t, ^3J(H,H) = 7.5 Hz, 7.0 Hz, 3H; δ-CH_3-Ile), 1.06, 1.08 (d, ^3J(H,H) = 6.5 Hz, 3H; γ-CH_3-Ile), 1.10, 1.12 (d, ^3J(H,H) = 6.5 Hz, 3H; γ-CH_3-Ile), 1.14–1.28 (m, 2H; γ-CH_2-Ile), 1.29, 1.30 (d, ^3J(H,H) = 6.0 Hz, 3H; γ-CH_3-Thr), 1.32, 1,34 (d, ^3J(H,H) = 6.5 Hz, 3H; γ-CH_3-Thr), 1.51–1.57 (m, 2H; γ-CH_2-Ile), 2.42–2.47 (m, 1H; β-CH-Ile), 2.65–2.66 (m, 1H; β-CH-Ile), 3.74–3.78 (dd, ^3J(H,H) = 7.5 Hz, 8.0 Hz, 1H; α-CH-Ile), 4.28–4.39 (4m, 5H; α-CH-Ile, CH_2-Gly, α-CH-Thr, β-CH-Thr), 5.10–5.15 (dd, ^3J(H,H) = 9.5 Hz, 9.5 Hz, 2H; CH_2-Gly), 7.64 (s, 1H; CH-Thz), 7.67 (s, 1H; CH-Thz), 7.82, 7.84 (d, ^3J(H,H) = 8.5 Hz, 1H; NH-Thr), 8.18, 8.19, 8.21 (t, ^3J(H,H) = 8.5 Hz, 8.0 Hz, 2H; NH-Gly), 8.71, 8.73 (d, ^3J(H,H) = 8.5 Hz, 1H; NH-Thr), 8.77, 8.78 (d, ^3J(H,H) = 7.0 Hz, 1H; NH-Ile), 9.49, 9.50 (d, ^3J(H,H) = 7.5 Hz, 1H; NH-Ile;); ESMS: *m*/*z* (%): 709.3 (100) $[M+H]^+$; HRMS: 709.27518, calcd for $C_{30}H_{45}N_8O_8S_2$ 708.28018; elemental analysis calcd (%) for $C_{30}H_{44}N_8O_8S_2 \cdot 3H_2O$: C 47.23, H 6.61, N 14.69; found C 47.23, H 6.07, N 14.44; retention time for analytical HPLC (gradient, 32 min.): 20.06 min.

Mononuclear copper(II) complexes of PatJ^1: To a 0.002 M solution of PatJ^1 (150 µL) in methanol was added one equivalent of a 0.019 M solution of $Cu(ClO_4)_2$ in methanol. To this mixture was added dropwise two equivalents of a 0.017 M solution of NaOH in methanol, and the resulting mixture was shaken after each addition. MS: *m*/*z* (%) (addition of two equivalents ofbase): $[H_6PatJ^1Na]^+ = 731.5$ (100), calcd 731.8; $[Cu(H_5PatJ^1)]^+ = 771.7$ (5), calcd 771.4; $[CuNa(H_4PatJ^1)]^+ = 792.4$ (8), calcd 793.5; $[Cu_2(H_3PatJ^1)]^+ = 831.4$ (3), calcd 832.9; $[Cu_2Na(H_2PatJ^1)]^+ = 853.3$ (20), calcd 854.9; negative ions: $[Cu(H_3PatJ^1)(H_2O)_2]^- = 805.9$ (18), calcd 805.4; $[Cu_2(H_1PatJ^1)]^- = 827.7$ (3), calcd 830.8; $[Cu_2(H_3L)(OH)_2]^- = 866.7$ (3), calcd 886.9; $[Cu_2(H_1PatJ^1)(MeOH)_3]^- = 927.6$ (3), calcd 926.7; for UV/Vis spectra see Table 1.

Dinuclear copper(II) complexes of PatJ^1: To a 0.002 M solution of PatJ^1 (150 µL) was added two equivalents of a 0.019 M solution of $Cu(ClO_4)_2$ in methanol. To this mixture was added dropwise six equivalents of a 0.017 M solution of NaOH in methanol, and the resulting mixture was shaken after each addition. MS: *m*/*z* (%) (addition of six equivalents of base): $[Cu_2Na(H_2PatJ^1)]^+ = 853.3$ (61), calcd 854.8; negative ions: $[Cu(H_3PatJ^1)]^- = 767.0$ (20), calcd 769.4; $[Cu_2(H_1PatJ^1)]^- = 827.8$ (42), calcd 830.8; $[Cu_2(PatJ^1)]^{2-} = 414.4$ (17), calcd 414.9; for UV/Vis spectra see Tables 1, 2.

Mononuclear copper(II) complexes of PatJ^2: To a 0.002 M solution of PatJ^1 (150 µL) in methanol was added one equivalent of a 0.019 M solution of $Cu(ClO_4)_2$ in methanol. To this mixture was added dropwise two equivalents of a 0.017 M solution of NaOH in methanol, and the resulting mixture was shaken after each addition. MS: m/z (%) (addition of two equivalents of base): $[H_6PatJ^2Na]^+ = 731.4$ (100), calcd 731.8; $[H_5PatJ^2Cu]^+ = 771.7$ (7), calcd 771.4; $[H_2PatJ^2Cu_2Na]^+ = 855.3$ (7), calcd 854.8; negative ions: $[H_3PatJ^2Cu(H_2O)_2]^- = 805.9$ (100), calcd 805.4; for UV/vis spectra see Table 1.

Dinuclear copper(II) compexes of PatJ^2: To a 0.002 M solution of PatJ^1 (150 µL) was added two equivalents of a 0.019 M solution of $Cu(ClO_4)_2$ in methanol. To this mixture was added dropwise six equivalents of a 0.017 M solution of NaOH in methanol, and the resulting mixture was shaken after each addition. MS: m/z (%) (addition of six equivalents of base): $[Na(H_6PatJ^2)]^+ = 731.5$ (100), calcd 731.8; $[CuNa(H_4PatJ^2)]^+ = 792.4$ (8), calcd 793.5; $[Cu_2Na(H_2PatJ^2)]^+ = 855.3$ (12),calcd 855.9; for UV/vis spectra, see Tables 1, 2.

The cyclic peptide PatL and the corresponding copper compounds were prepared and characterized analogously, see Supporting Information.

Acknowledgement

Financial support by the German Science Foundation (DFG) is gratefully acknowledged.

[1] J. P. Michael, G. Pattenden, *Angew. Chem.* **1993**, *105*, 1; *Angew. Chem. Int. Ed. Engl.* **1993**, *32*, 1.
[2] J. R. Lewis, *Natural Products Report* **1989**, *6*, 503.
[3] D. Faulkner, *J. Nat. Prod. Rep.* **1988**, 613.
[4] H. C. Krebs, *Fortschr. Chem. Org. Naturst.* **1986**, *49*, 151.
[5] D. P. Fairlie, G. Abbenante, D. M. March, *Curr. Med. Chem.* **1995**, *2*, 672.
[6] M. K. Rosen, S. L. Schreiber, *Angew. Chem.* **1992**, *104*, 413; *Angew. Chem. Int. Ed. Engl.* **1992**, *31*, 384.
[7] D. A. Evans, J. A. Ellman, *J. Am. Chem. Soc.* **1991**, *113*, 1063.
[8] N. Fusetani, T. Sugawara, S. Matsunaga, *J. Am. Chem. Soc.* **1991**, *113*, 7811.

[9] A. L. van den Brenk, PhD thesis, University of Queensland (Australia), **1994**.
[10] D. Baron, L. G. Pease, E. R. Blout, *J. Am. Chem. Soc.* **1977**, *99*, 8299.
[11] C. H. Nin, V. Madison, L. G. Pease, E. R. Blout, *Biopolymers* **1978**, *17*, 2747.
[12] H. Miyake, Y. Kojima, *Coord. Chem. Rev.* **1996**, *148*, 301.
[13] A. L. van den Brenk, K. A. Byriel, D. P. Fairlie, L. R. Gahan, G. R. Hanson, C. J. Hawkins, A. Jones, C. H. L. Kennard, B. Moubaraki, K. S. Murray, *Inorg. Chem.* **1994**, *33*, 3549.
[14] L. Grondahl, N. Sokolenko, G. Abberate, D. P. Fairlie, G. R. Hanson, L. R. Gahan, *J. Chem. Soc. Dalton Trans.* **1999**, 1227.
[15] D. J. P. Freeman, A. F. Drake, G. Siligardi, *J. Chem. Soc. Perkin Trans. 2* **1998**, 129.
[16] L. A. Morris, M. Jaspars, J. J. K.-v. d. Bosch, K. Versluis, A. J. R. Heck, S. M. Kelly, N. C. Price, *Tetrahedron* **2001**, *57*, 3185.
[17] L. A. Morris, B. F. Milne, M. Jaspars, J. J. K.-v. d. Bosch, K. Versluis, A. J. R. Heck, S. M. Kelly, N. C. Price, *Tetrahedron* **2001**, *57*, 3199.
[18] A. L. van den Brenk, D. P. Fairlie, G. R. Hanson, L. R. Gahan, C. J. Hawkins, A. Jones, *Inorg. Chem.* **1994**, *33*, 2280.
[19] A. L. van den Brenk, D. P. Fairlie, L. R. Gahan, G. R. Hanson, T. W. Hambley, *Inorg. Chem.* **1996**, *35*, 1095.
[20] G. Abbenante, D. P. Fairlie, L. R. Gahan, G. R. Hanson, G. K. Pierens, A. L. van den Brenk, *J. Am. Chem. Soc.* **1996**, *118*, 10384.
[21] P. Comba, R. Cusack, D. P. Fairlie, L. R. Gahan, G. R. Hanson, U. Kazmaier, A. Ramlow, *Inorg. Chem.* **1998**, *37*, 6721.
[22] T. Ishida, M. Tanaka, M. Nabae, M. Inoue, S. Kato, Y. Hamada, T. Shioiri, *J. Org. Chem.* **1988**, *53*, 107.
[23] T. Ishida, Y. In, F. Shinozaki, M. Doi, D. Yamamoto, Y. Hamada, T. Shioiri, M. Kamigauchi, M. Sugiwra, *J. Org. Chem.* **1995**, *60*, 3944.
[24] M. P. Foster, G. P. Concepcion, G. B. Caraan, C. M. Ireland, *J. Org. Chem.* **1992**, *57*, 6671.
[25] J. D. White, W. K. M. Chong, K. Thirring, *J. Org. Chem.* **1983**, *48*, 2302.
[26] H. Morita, N. Yoshida, K. Takeya, H. Itokawa, O. Shirota, *Tetrahedron* **1996**, *52*, 2795.
[27] F. J. Schmitz, M. B. Ksebati, J. S. Chang, J. L. Wang, M. B. Hossain, D. van der Helm, *J. Org. Chem.* **1989**, *54*, 3463.
[28] R. M. Cusack, L. Grondal, G. Abbenante, D. P. Fairlie, L. R. Gahan, G. R. Hanson, T. W. Hambley, *J. Chem. Soc. Perkin Trans. 2* **2000**, 323.
[29] P. V. Bernhardt, P. Comba, T. W. Hambley, S. S. Massoud, S. Stebler, *Inorg. Chem.* **1992**, *31*, 2644.
[30] P. Comba, *Comm. Inorg. Chem.* **1994**, *16*, 133.
[31] P. Comba, T. W. Hambley, P. Hilfenhaus, D. T. Richens, *J. Chem. Soc. Dalton Trans.* **1996**, 533.
[32] P. Comba, P. Hilfenhaus, *J. Chem. Soc. Dalton Trans.* **1995**, 3269.
[33] D. Wang, G. R. Hanson, *Appl. Magn. Reson.* **1996**, *11*, 401.
[34] D. Wang, G. R. Hanson, *J. Magn. Reson. A* **1995**, *117*, 1.
[35] M. Griffin, A. Muys, C. Noble, D. M. Wang, C. Eldershaw, K. E. Gates, K. Burrage G. R. Hanson, *Mol. Phys. Rep.* **1999**, *26*, 60.
[36] J. Bartol, P. Comba, M. Melter, M. Zimmer, *J. Comput. Chem.* **1999**, *20*, 1549.
[37] T. Ishida, Y. In, M. Doi, M. Inoue, Y. Hamada, T. Shiori, *Biopolymers* **1992**, *32*, 131.
[38] T. D. Smith, J. R. Pilbrow, *Coord. Chem. Rev.* **1974**, *13*, 173.
[39] P. Comba, T. W. Hambley, N. Okon, G. Lauer, *MOMEC97, a molecular modeling package for inorganic compounds,* CVS, Heidelberg, **1997**.
[40] J. E. Bol, C. Buning, P. Comba, J. Reedijk, M. Ströhle, *J. Comput. Chem.* **1998**, *19*, 512.
[41] G. M. Sheldrick, *Acta Crystallogr. Sect. A* **1990**, *46*, 467.
[42] G. M. Sheldrick, *University of Göttingen*, **1993**.
[43] C. K. Johnson, ORTEP, A Thermal Ellipsoid Plotting Program, Oak Ridge National Laboratories, Oak Ridge, TN, **1965**.

Received: September 26, 2001 [F3576]

  0947-6539/02/0807-1536 $ 20.00+.50/0